HHS Public Access

Author manuscript

Acta Biomater. Author manuscript; available in PMC 2015 June 01.

Published in final edited form as:

Acta Biomater. 2014 June ; 10(6): 2473–2481. doi:10.1016/j.actbio.2014.02.024.

Translation of an Engineered Nanofibrous Disc-like Angle Ply Structure for Intervertebral Disc Replacement in a Small Animal Model

John T. Martin, M.S.[a,b,e], **Andrew H. Milby, M.D.**[a,e], **Joseph A. Chiaro**[a,e], **Dong Hwa Kim, Ph.D.**[a], **Nader M. Hebela, M.D.**[a,e], **Lachlan J. Smith, Ph.D.**[a,e,f], **Dawn M. Elliott, Ph.D.**[c], and **Robert L. Mauck, Ph.D.**[a,b,d,e,*]

[a]Department of Orthopaedic Surgery, University of Pennsylvania, McKay Orthopaedic Research Laboratory, 36th Street and Hamilton Walk, 424 Stemmler Hall, Philadelphia, PA, USA 19104-6081

[b]Department of Mechanical Engineering and Applied Mechanics, University of Pennsylvania, 220 South 33rd Street, 229 Towne Building, Philadelphia, PA, USA 19104-6315

[c]Department of Biomedical Engineering, University of Delaware, 125 E. Delaware Avenue, Newark, DE, USA 19716

[d]Department of Bioengineering, University of Pennsylvania, 210 South 33rd Street, Suite 240 Skirkanich Hall, Philadelphia, PA, USA 19104-6321

[e]Translational Musculoskeletal Research Center, Philadelphia VA Medical Center, 3900 Woodland Avenue, Building 21, Room A200, Philadelphia, PA, 19104

[6]Department of Neurosurgery, University of Pennsylvania, 3400 Spruce Street, 3rd Floor Silverstein Pavilion, Philadelphia, PA 19104

Abstract

Intervertebral disc degeneration has been implicated in the etiology of low back pain; however the current surgical strategies for treating symptomatic disc disease are limited. A variety of materials have been developed to replace disc components, including the nucleus pulposus (NP), the annulus fibrosus (AF), and their combination into disc-like engineered constructs. We have previously shown that layers of electrospun poly(ε-caprolactone) scaffold, mimicking the hierarchical organization of the native AF, have functional parity with native tissue. Likewise, we have combined these structures with cell-seeded hydrogels (as an NP replacement) to form disc-like angle ply structures (DAPS). The objective of this study was to develop a model for the evaluation of DAPS *in vivo*. Through a series of studies, we developed a surgical approach to replace the rat caudal disc with an acellular DAPS and then stabilize the motion segment by external fixation. We then optimized cell infiltration into DAPS by including sacrificial

[*]**Corresponding Author:** Robert L. Mauck, Ph.D., Associate Professor of Orthopaedic Surgery and Bioengineering, University of Pennsylvania, McKay Orthopaedic Research Laboratory, 36th Street and Hamilton Walk, 424 Stemmler Hall, Philadelphia, PA 19104-6081, Phone: 215-898-3294, lemauck@mail.med.upenn.edu.

Disclosures

The authors have no potential conflicts of interest.

poly(ethylene oxide) layers interspersed throughout the angle-ply structure. Our findings illustrate that DAPS are stable in the caudal spine, are infiltrated by cells from the peri-implant space, and that infiltration is expedited by providing additional routes for cell migration. These findings establish a new *in vivo* platform in which to evaluate and optimize the design of functional disc replacements.

Keywords

Intervertebral Disc; Tissue Engineering; Electrospinning; Surgical Model; External Fixation

1. Introduction

Chronic low back pain affects over 50% of the population aged 65 or younger, and prevalence increases with age [1], resulting in more than $100 billion in medical costs and lost wages in the United States. [2] Lumbar intervertebral disc degeneration has been implicated as a causative factor in low back pain, and deficiency in disc function is closely tied to the degeneration of its components. [3–5] Current surgical strategies for treating symptomatic disc degeneration, including spinal fusion and total disc arthroplasty, do not restore native joint mechanics and are associated with downstream complications. For example, fusion of a lumbar motion segment limits mobility and may accelerate adjacent segment degeneration [6], while prosthetic discs are subject to subsidence and migration, with limited benefit in comparison to fusion. [7, 8] Thus, the role of these interventions in treating low back pain is controversial and continues to evolve.

A number of therapeutic strategies have been developed for each stage of the degenerative process to preserve or restore function of the intervertebral joint. Early in the degenerative process, interventions with cell, gene, or pharmaceutical therapies may maintain disc function by reducing inflammation and preventing further matrix degradation. [9–11] A more substantial approach will likely be necessary for the treatment of end-stage disc disease, due to depletion of the endogenous cell population and irreversible deterioration of tissue structure. In such circumstances, a composite (or whole disc) approach would be required, where the entirety of disc structure and function is replicated. Towards that end, a number of studies have reported on co-cultured NP and AF components for tissue-engineered total disc replacement. These cell-seeded engineered discs have been evaluated *in vitro* [12, 13], in the subcutaneous space [14–16], and have recently been placed *in situ* between rat lumbar and caudal vertebrae [17, 18], illustrating the rapid advances in this regenerative approach to engineered disc replacement.

Current engineered discs do not replicate the hierarchical AF organization required to support multiaxial spinal loads. The AF is comprised of lamellae, discrete fibrous sheets with specialized collagen alignment. Within each lamella, fibers run in a single direction, ranging from 20° to 50° with respect to the transverse plane, and adjacent lamellae have opposing fiber orientation, producing an angle-ply structure. [19] Multi-directional load-bearing during compression, torsion, flexion/extension, lateral bending, and shear is supported by tensile reinforcement provided by fibers oriented in these directions. [20] An

engineered disc may need to incorporate aspects of this native design for proper function of the regenerated tissue.

We have previously used electrospinning to generate engineered materials that recreate the organized fibrous architecture of the native AF. [21–25] Electrospun scaffolds with aligned nanofibers permit cell attachment and promote directed matrix production for reinforcement in principal loading directions. [26–28] Specifically, electrospun poly(ε-caprolactone) (PCL) seeded with either AF cells or mesenchymal stem cells increases in functional properties with *in vitro* culture, approaching native tissue properties at the single and multi-lamellar length scales. [21, 22, 28] Single strips of aligned scaffold can be arranged concentrically, precisely mimicking the alternating fiber alignment of native tissue, to form disc-like angle ply structures (DAPS). [24] Like their single layer counterparts, these constructs mature both compositionally and mechanically over time in culture, indicating their potential for use in total disc replacement.

The objective of this study was to develop a disc replacement model in which to evaluate DAPS *in vivo*. The murine caudal spine, used in many disc studies to investigate degenerative processes [5, 29] and engineered disc replacements [30, 31], is an ideal candidate for preclinical studies given the ease of surgical access and the ability to avoid critical structures (e.g., spinal cord and spinal nerves). In the context of disc tissue engineering, the rat tail model serves as a high-throughput system to screen engineered disc designs and inform large animal studies. Thus, we developed a rat tail disc replacement model in which native caudal discs were removed and replaced with the electrospun AF-region of engineered DAPS. Here, our focus on the AF was to specifically assess the potential for colonization of and matrix deposition in electrospun scaffolds in the *in vivo* disc environment. Given early findings of graft displacement, we also developed an external fixation system to stabilize the disc space. Further, since early studies showed poor infiltration of the AF region of the DAPS by endogenous cells, we included sacrificial layers within the DAPS structure to provide additional routes for cell migration.

2. Materials and Methods

2.1 Preparation of Disc-like Angle Ply Structures (DAPS)

DAPS were fabricated to reproduce the hierarchical structure of the native AF (Fig. 1A, B). [24] Aligned nanofibrous sheets (thickness = 250 μm) were formed by electrospinning a 14.3% w/v solution of PCL (Shenzhen BrightChina Industrial Co., Hong Kong, China) dissolved in a 1:1 mixture of tetrahydrofuran (THF) and N,N-dimethylformamide (DMF) (Fisher Chemical, Fairlawn, NJ) (Fig. 1C). The polymer solution was extruded at a rate of 2.5 mL/hour through a 13 kV-charged 18G needle. Fibers were drawn across a 15 cm air gap onto a grounded mandrel rotating with a surface velocity of 10 m/s. The resultant sheets of aligned nanofibers were cut into strips with fibers aligned at 30° relative to the strip long axis to mimic the native AF fiber architecture (Fig. 1D). [22, 24] Two strips with opposing fiber orientation were wrapped concentrically and fixed with a spot weld to form the AF region of the DAPS (Fig. 1E).

Preliminary characterization of DAPS fabricated in this manner included the measurement of DAPS geometry and compressive mechanical properties (n=7). First, a non-contact laser device was used to measure height [32] and images of DAPS were taken with a digital camera and processed in Matlab to determine inner and outer diameters. [33] DAPS were then tested in unconfined compression on an electromechanical testing system (Instron 5542, Instron, Norwood, MA). First, a 0.5 N preload was applied and allowed to relax over 300 s. Next, three consecutive compressive strain ramps of 5% magnitude were applied with a 300 s relaxation period between each ramp. The compressive equilibrium modulus was defined as the slope of a line fit through points at equilibrium after 5%, 10%, and 15% strain. The mean DAPS dimensions were: 5.1±0.4 mm outer diameter, 1.0±0.1 mm inner diameter, and 1.9±0.3 mm height. These dimensions allow a press-fit into the (caudal) C8/C9 disc space and are comparable to the native rat caudal disc geometry (4.15 mm outer diameter, 2 mm NP diameter, 0.94 mm height [34]). The compressive equilibrium modulus was 12.6±4.3 kPa and was lower than that of the native rat caudal disc (238 kPa [17]), but was expected to increase after implantation as cells infiltrate and deposit a collagenous matrix.

2.2 Surgical Implantation of DAPS into the Rat Caudal Spine

In a first set of surgeries, DAPS consisting of only the AF region were implanted into the caudal spines of Sprague Dawley rats (male, 7–9 months, 478±11g) in accordance with local institutional regulations. Rats were first anesthetized and, using the sacrum as an anatomical landmark, the (caudal) C8 and C9 vertebral bodies were located via fluoroscopy (Orthoscan HD, Orthoscan, Inc., Scottsdale, AZ). Then, the dorsal skin spanning the vertebral bodies was incised, the dorsal tendons were partially separated from their bony insertions adjacent to the C8/C9 disc with a scalpel, and the native disc was removed. A double-armed non-absorbable suture was passed through the DAPS center, fed through the disc space, and tied exterior to the ventral skin to anchor the implant in place (Fig. 2A). The incision was then closed with non-absorbable simple interrupted sutures. Post-surgical management included prophylactic treatment of infection (cefazolin, 15 mg/kg subcutaneous, 1 day pre-op and 2 days post-op), inflammation (meloxicam, 1 mg/kg subcutaneous, 1 day post-op), and pain (buprenorphine, 0.1 mg/kg subcutaneous, 3 days post-op). Rats were returned to normal cage activity and euthanized at either 14 (n=6) or 28 days (n=9). Additional rats were assigned to a discectomy-only control group, in which the native disc was removed in its entirety but no implant was placed. These rats were also euthanized at 14 (n=4) or 28 days (n=4).

2.3 Evaluation of Disc Height

To evaluate implant stability, caudal spines were imaged fluoroscopically pre-operatively, immediately post-operatively and at regular intervals through 28 days (Fig. 2B). Disc height index (DHI) [35], a standard technique used to normalize disc height to vertebral body length, was quantified from lateral fluoroscopic images using a custom Matlab program (Fig. 2C). The disc and adjacent vertebral bodies areas (A_{VB1}, A_{VB2}, A_D) and widths (W_{VB1}, W_{VB2}, W_D) were quantified digitally. The mean vertebral body lengths (L_{VB1}, L_{VB2}) were defined as $L_{VB} = A_{VB}/W_{VB}$, the disc height (H_D) as $H_D = A_D/W_D$, and DHI as $DHI = 2H_D/(L_{VB1}+L_{VB2})$. For longitudinal analysis, DHI was expressed as a percentage of pre-operative

DHI (%DHI_0). Implants were deemed ‘successful’ if 75% DHI_0 was maintained at the terminal timepoint and ‘displaced’ if this was not the case.

2.4 Microcomputed Tomography (μCT)

To assess disc height and adjacent vertebral bone remodeling, μCT scans (vivaCT 75, SCANCO Medical AG, Bruttisellen, Switzerland) of the caudal spine were acquired after euthanasia at an isotropic resolution of 20.5 μm. Three-dimensional reconstructions were generated for visualization of the disc space and bony surfaces.

2.5 DAPS Implantations with External Fixation

Several DAPS were displaced from the intervertebral space in the initial surgical series; likely due to the eccentric loading conditions in the caudal spine. This motivated development of an external fixation system to improve implant retention. A radiolucent PEEK/stainless steel ring-type external fixator [36] was designed to unload and stabilize the intervertebral space (Fig. 3A). To apply the fixator, 0.8 mm Kirschner wires (Synthes Inc., West Chester, PA) were passed laterally through the mid-height of the C8 and C9 vertebral bodies with a pneumatic wire driver, the ‘C’ shaped rings of the fixator were slid onto the wires ventrally leaving access to the dorsal tail, and the intervertebral height was set by adjusting the position of nuts on the threaded rods. With the fixator in place, removal of the native disc and DAPS implantations proceeded as described above, though no internal suture was used to secure the DAPS (Fig. 3B). Rats received the same pre- and post-surgical medication regimen and were returned to normal cage activity until euthanasia at 14 (n=4) or 28 days (n=5). An additional external fixator plus discectomy control group was included to verify preservation of disc height with application of the fixator at 14 (n=2) and 28 days (n=4). Rats from all external fixator surgeries were subjected to serial fluoroscopy (Fig. 3C) and μCT (after the fixator was removed) as described above.

To facilitate regular assessment of the position of implanted DAPS, radiopaque DAPS (rDAPS) were fabricated to enable visualization via fluoroscopy. To do so, PCL solutions were supplemented with the radiopaque nanopowder, zirconia (Zirconium(IV) Oxide Nanopowder, Sigma-Aldrich, St. Louis, MO). Nanofibrous radiopaque sheets (thickness = 250 μm) were formed by electrospinning a 14.3% w/v solution of 50% PCL and 50% zirconia dissolved in a 1:1 mixture of THF and DMF. To monitor changes of implant position over time, rDAPS were implanted along with application of the external fixator described above (Fig. 3D). Rats with rDAPS were subject to serial fluoroscopy and euthanized at 28 days for μCT (n=2).

2.6 Histological Analysis

All segments from DAPS, fixation+DAPS, discectomy, and fixation+discectomy surgeries were fixed in buffered formalin and decalcified in formic acid. Vertebra-DAPS-vertebra motion segments were sectioned to 30 μm thickness in the dorsoventral plane on a cryostat microtome (Microm HM 500, Thermo Scientific, Waltham, MA). Sections were stained with hematoxylin and eosin (H&E) to visualize cell infiltration and matrix deposition. Stained sections were observed and imaged under bright field with an upright microscope (Eclipse 90i, Nikon, Tokyo, Japan). Additional samples were imaged with cross-polarized

light to inspect the DAPS lamellar structure. Sections were also stained with 4',6-diamidino-2-phenylindole (DAPI) to visualize cell nuclei; these samples were imaged under fluorescence and overlaid with differential interference contrast (DIC) microscopy images to highlight the location of cells with respect to the DAPS lamellar structure.

2.7 Implantation of DAPS with Sacrificial Layers to Improve Cell Infiltration

After the achievement of implant stability, the slow migration of endogenous cells into the PCL-only DAPS warranted the modification of the scaffold material to include routes for cell infiltration. Sacrificial layer DAPS (sDAPS) were fabricated by sequentially electrospinning two layers of polymer, the first, a standard aligned PCL layer, and the second, a water soluble poly(ethylene oxide) (PEO) layer (200kDa, Polysciences, Inc., Warrington, PA). PEO nanofibers were electrospun from a 10% w/v solution of PEO dissolved in 90% ethanol. This solution was drawn through an 18G needle across a 10 kV gradient at 2.5 mL/hr and collected onto the rotating mandrel atop the deposited PCL layer. Strips were cut from the composite PCL/PEO mats and wrapped using the same method as described above, forming sDAPS.

To evaluate infiltration, sDAPS were first seeded *in vitro* with bovine AF cells and cultured for 7 days (Fig. 7A). For this, a 31G needle was passed radially through the mid-height of the sDAPS to stabilize the structure. The sDAPS were then rehydrated in a series of gradient ethanol washes to remove PEO layers and coated overnight in a solution containing 20 μg/mL fibronectin (Sigma-Aldrich, St. Louis, MO) to improve cell attachment. [37] The sDAPS were then lyophilized and seeded with passage 2 bovine AF cells isolated as described previously. [23] Cells were loaded onto each surface (1×10^6 cells per side) and allowed to incubate for 1 hour per side before culture in media containing Dulbecco's modified Eagle's medium (Gibco, Invitrogen Life Sciences, Carlsbad, CA), 1% penicillin, streptomycin, and fungizone (Gibco), and 10% fetal bovine serum (Gibco) for 7 days. Three types of DAPS were included in the study (n = 3/constructs/group); PCL only DAPS (250 μm layer thickness), 'thick' sDAPS (125 μm PCL layer, 250 μm PEO layer), and 'thin' sDAPS (125 μm PCL layer, 125 μm PEO layer). Infiltration was evaluated by DAPI staining of cross sections on day 7, as described above.

Acellular sDAPS, with *intact* thick or thin PEO layers, were also implanted into the rat caudal spine (using the external fixator), and cell infiltration was evaluated after 14 days *in vivo* (n=3/group) (Fig. 7A). Following euthanasia, motion segments were sectioned, stained with H&E or picrosirius red (for collagen), and imaged by brightfield or polarized light microscopy.

2.8 Statistical Analysis

DHI was statistically assessed by grouping discectomy, displaced DAPS, successful DAPS, fixation+discectomy and fixation+DAPS surgeries and implementing an ANOVA, with comparisons made among groups within each timepoint and to pooled pre-operative measurements. Tukey's post-hoc test was used for pairwise comparisons ($p<0.05$). Statistical analyses were performed using Prism 5 (GraphPad Software Inc., La Jolla, CA).

3. Results

3.1 DAPS Implantations in the Caudal Spine

DAPS implantations using only a suture anchor successfully maintained 75% DHI_0 in 8 of 15 surgeries (Fig. 4A). Immediately after implantation, an increase in DHI was noted following the press-fit of DAPS into the disc space. DHI gradually decreased over time, but, by day 28, DHI for successful implants was not different from pre-operative DHI. Following discectomy alone, the disc space also initially expanded, likely due to joint laxity caused by detachment of the dorsal tendon bundles, but collapsed to 40% of preoperative DHI by 28 days. In cases where DAPS were displaced from the intervertebral space, there was variability in the timing of implant failure, as evidenced by large standard deviations of DHI at 14 days in the displaced group. However, by day 28, there was no difference in DHI between the displaced DAPS and discectomy groups. Gross examination of tails from the displaced DAPS group revealed that the DAPS were located in the dorsal subcutaneous space at both the 14 and 28 day timepoints.

3.2 External Fixation Preserves Disc Height

External fixation caused no changes in surgical outcome or post-operative cage activity. All DAPS implanted with external fixation remained in the disc space for the duration of the study. With the fixation system in place, disc height was preserved, even in the case of discectomy. At day 14 and 28, the fixation+discectomy DHI was significantly greater than the discectomy-only DHI, and was not different from pre-operative levels. DHI was also maintained by external fixation in all fixation+DAPS surgeries; $\%DHI_0$ post-op was set at 165% to allow room for DAPS implantation. This was significantly different from pre-operative DHI and remained so through day 28.

3.3 Vertebral Bone Morphology Post-DAPS Implantation

Reconstructions of μCT scans confirmed the maintenance of disc height in successful DAPS surgeries and the collapse of disc height in displaced DAPS and discectomy surgeries at 28 days (Fig. 4B). In the discectomy group, the intervertebral space collapsed, though there was no evidence of adjacent vertebral bone remodeling. Conversely, in the displaced DAPS group, bone remodeling was present adjacent to the collapsed disc space, though the reason for this new bone deposition is unclear. In successful DAPS surgeries, the intervertebral space was intact, and minor misalignment and remodeling were evident in all cases. External fixation prevented collapse with minimal superficial bone deposition at the K-wire insertion sites as illustrated in the both fixation groups. Reconstructions of rDAPS confirmed intervertebral positioning at 28 days (Fig. 4B).

3.4 Histological Appearance of DAPS and the Intervertebral Space

Histological analysis via H&E staining confirmed that disc height was maintained by the external fixator, even following discectomy, and that in all 9 fixation+DAPS surgeries, the DAPS remained in the intervertebral space. In the absence of fixation, disc height collapsed following discectomy, with remnant AF visible at both timepoints (Fig. 5A, B). With the external fixator, the space left vacant by discectomy was partially filled with fibrous repair

tissue by 28 days (Fig. 5C, D). In fixation+DAPS surgeries, the DAPS remained in the intervertebral space at both 14 and 28 days (Fig. 5E, F), however, there was intense nuclear staining at the implant periphery with little or no matrix deposition between layers. Polarized light images of the H&E stained sections demonstrated that the lamellar structure (with alternating fiber angles) was intact over the course of the experiment (Fig. 5G, H). DAPI staining confirmed that few cells had infiltrated the AF structure of the DAPS, with nuclei confined primarily to the boundaries of the implant and few in the interlamellar space by day 28 (Fig. 6A). Cells that infiltrated had nuclei that were elongated, suggesting their interaction with the aligned nanofiber pattern (Fig. 6B).

3.5 Improved Colonization of sDAPS

sDAPS effectively maintained interlayer gaps for cell infiltration both *in vitro* and *in vivo*. In *in vitro* studies, AF cells penetrated the full height of both thick and thin PEO layer sDAPS after a one week culture period (Fig. 7C, D). Consistent with *in vivo* findings above, PCL-only DAPS were poorly infiltrated, with central areas completely devoid of cells (Fig. 7B). When implanted in the caudal disc space, sDAPS remained in place and maintained their structure over time (Fig. 7E, H). Along with advanced cell infiltration relative to PCL-only DAPS, collagen deposition was apparent between the remnant PCL layers, as evidenced by positive staining in both H&E (Fig. 7F, G) and picrosirius red sections (Fig. 7I, J). Furthermore, layers with alternating fiber orientation remained intact (Fig. 7I, J).

4. Discussion

Cell-based disc implants may enable reconstruction of the intervertebral disc with an engineered tissue that has the capacity to function as a living disc replacement. To further this goal, we engineered DAPS (with an AF region mirroring the hierarchical organization of the native disc), and evaluated their performance in an *in vivo* model of disc replacement in the rat caudal spine. This study was the first to assess an engineered disc that possessed a lamellar structure and fiber alignment similar to the native AF *in vivo*. In addition, we developed an external fixation system to stabilize the implant site and prevent implant extrusion, and further improved the DAPS by including sacrificial layers in the AF to improve upon poor endogenous cell infiltration.

This work validated the rat tail as a demanding, load-bearing model for disc replacement. While the axial loads experienced in the tail may be lower than the lumbar spine, the large angular displacements that occur during tail flexion (coincident with dynamic balancing activities) lead to graft displacement. Thus, in the absence of external fixation, DAPS were retained in the disc space in only 47% of surgeries, while with fixation 100% retention was achieved. Previous studies have demonstrated that a cell-seeded engineered composite disc comprised of a collagen hydrogel-based AF and an alginate hydrogel-based NP were retained in the rat lumbar and caudal disc space *without* external fixation. [17, 18] Differences in outcomes between that study and the current one may be due to differences in surgical approach, including the length of the dorsal skin incision, the treatment of dorsal tendon bundles, and the amount of annulus removed. Differences may also be due to the physical properties of the construct, where DAPS are ~4-fold stiffer in compression than the

collagen/alginate implants [38], perhaps making them more likely to displace (rather than compress) with tail flexion. Future studies could challenge such implants in a physiologic loading environment, with compressive loading and smaller angular displacements, like the lumbar or cervical spine. Alternatively, the rat caudal disc space could be subjected to controlled physiologic loads by modifying the external fixator to apply static or dynamic compressive forces. [36, 39] Such mechanical perturbation may act to increase biosynthetic activities in the implant, and encourage integration with the surrounding tissue. [39–42]

Another observation in this study was poor infiltration of endogenous cells, even in DAPS that were stably fixed in the disc space. Poor cell infiltration is a common drawback of electrospun scaffolds used for tissue engineering [43–46] and may have been exacerbated in this case by the tight wrapping of concentric layers during DAPS fabrication. Stable PCL-only DAPS showed poor infiltration over 28 days, with an accumulation of cells at the implant periphery and little or no matrix deposition between layers. This result was independent of external fixation (i.e., fibrous encapsulation was similar in successful PCL-only DAPS with or without an external fixator) and may be a limitation of that scaffold formulation. Nevertheless, stable retention of an implant, as is enabled by an external fixator, may improve or hasten integration by preventing micromotion that would interrupt newly formed tissue bridges. Borrowing from our previous work using PEO as a water-soluble porogen, we fabricated sDAPS with a sacrificial layer interwoven between PCL layers. This allowed for rapid and complete infiltration by cells *in vitro* and *in vivo*, as well as marked collagen deposition between layers. Future work will confirm the cell type responsible for this new tissue formation, and its composition.

Our goal in initiating these studies with an acellular, AF-only DAPS was to determine the viability of the caudal disc replacement model using such materials. However, acellular biomaterials have come to the fore in the context of tissue engineering as an alternative to cell-based methods. Acellular approaches are motivated by difficulties with cell isolation, handling, and behavior, and the regulatory obstacles that may act as barriers to clinical translation of biological therapies. [47] Here, we developed a material-based (rather than a cell-based) approach in which the AF construct is populated by active endogenous cells that secrete extracellular matrix proteins to produce functional tissue. This approach requires evaluation in the target patient population, whose degenerated disc environment (with deficient vascularity, low cellularity and chronic inflammation) might limit the capacity of endogenous cells to produce functional tissue. Our *in vitro* data also show that DAPS can be readily pre-seeded with exogenous cells (AF cells or mesenchymal stem cells) and coupled to an acellular or cell-based NP replacement to enable total disc replacement in such scenarios.

The interface between the DAPS and the adjacent soft tissue/vertebral bodies is critical for functional restoration of the motion segment but was not specifically evaluated in this study. Integration did occur with the surrounding soft tissue, as endogenous cells transited into sacrificial layer DAPS and deposited new extracellular matrix. Soft tissue contiguity was observed histologically, particularly in those implants with sacrificial layers that were more fully invested. This soft tissue bridge is likely quite fragile at early timepoints and thus future studies are required to mechanically evaluate the forming interface as a function of

time as matrix deposition continues. It is also likely that additional steps must be taken to specifically enhance integration, and this model provides a platform to optimize both implant design and surgical strategy to promote implant integration within the motion segment.

A primary limitation of this model is the use of external fixation to unload the disc space, and so implants were not challenged or modulated by the physiologic loading environment. The current fixator design can, however, be modified to enable application of controlled static or dynamic loads. [36, 39, 48] Thus, this model provides an opportunity to investigate how the mechanical boundary conditions alter integration at the vertebral interface and guide maturation of the DAPS. Additionally, we excluded major disc structures, namely the NP and the cartilaginous/vertebral endplates, to focus on model development and the improvement of the AF region of the DAPS. Future implant design will involve DAPS inclusive of an NP region to form a composite total disc replacement.

5. Conclusion

This study advances the goal of biologic total disc replacement by validating a rat caudal spine model for *in vivo* testing of engineered disc replacements, and illustrates that a stable fixation system improves the retention of implanted discs. We evaluated the performance of a nanofibrous scaffold that was structurally equivalent to the native AF and found that the dense PCL scaffold formed by electrospinning did not permit endogenous cell infiltration. However, by modifying the design to include water soluble layers to create interlamellar spaces, endogenous cells populated the full thickness of the implant and produced a collagenous network. Future work will build upon this foundation to further the goal of a functional, tissue-engineered total disc replacement.

Acknowledgements

We would like to thank the exceptional staff of the Philadelphia VA Medical Center Animal Research Facility: Debra Pawlowski, Jeffrey House, and Pierina Deritis. In addition we like to thank Deborah Gorth and Feini Qu (animal procedures), Alexei Adan (DAPS fabrication and histology), Subash Poudel (DAPS geometry and mechanical property measurements), Sophia Stylianos (fabrication of surgical equipment), and Dr. Thomas Schaer (sterilization facilities). This work was funded by the Department of Defense (Grant #OR090090) and the Department of Veterans Affairs (Grant# I01RX000211).

References

1. Andersson GB. Epidemiological features of chronic low-back pain. Lancet. 1999; 354:581–585. [PubMed: 10470716]
2. Katz JN. Lumbar Disc Disorders and Low-Back Pain: Socioeconomic Factors and Consequences. The Journal of Bone & Joint Surgery. 2006; 88-A(Supplement 2):21–24. [PubMed: 16595438]
3. Hsieh AH, Hwang D, Ryan DA, Freeman AK, Kim H. Degenerative anular changes induced by puncture are associated with insufficiency of disc biomechanical function. Spine (Phila Pa 1976). 2009; 34:998–1005. [PubMed: 19404174]
4. O'Connell GD, Vresilovic EJ, Elliott DM. Human intervertebral disc internal strain in compression: the effect of disc region, loading position, and degeneration. J Orthop Res. 29:547–555. [PubMed: 21337394]

5. Martin JT, Gorth DJ, Beattie EE, Harfe BD, Smith LJ, Elliott DM. Needle puncture injury causes acute and long-term mechanical deficiency in a mouse model of intervertebral disc degeneration. J Orthop Res. 2013; 31:1276–1282. [PubMed: 23553925]
6. Helgeson MD, Bevevino AJ, Hilibrand AS. Update on the evidence for adjacent segment degeneration and disease. Spine J. 2013; 13:342–351. [PubMed: 23420004]
7. van den Eerenbeemt KD, Ostelo RW, van Royen BJ, Peul WC, van Tulder MW. Total disc replacement surgery for symptomatic degenerative lumbar disc disease: a systematic review of the literature. Eur Spine J. 2010; 19:1262–1280. [PubMed: 20508954]
8. Costi JJ, Freeman BJC, Elliott DM. Intervertebral disc properties: challenges for biodevices. Expert Rev Med Devic. 2011; 8:357–376.
9. Masuda K. Biological repair of the degenerated intervertebral disc by the injection of growth factors. Eur Spine J. 2008; 17(Suppl 4):441–451. [PubMed: 19005698]
10. Woods BI, Vo N, Sowa G, Kang JD. Gene therapy for intervertebral disk degeneration. Orthop Clin North Am. 2011; 42:563–574. ix. [PubMed: 21944592]
11. Huang YC, Leung VY, Lu WW, Luk KD. The effects of microenvironment in mesenchymal stem cell-based regeneration of intervertebral disc. Spine J. 2013; 13:352–362. [PubMed: 23340343]
12. Park SH, Gil ES, Cho H, Mandal BB, Tien LW, Min BH, et al. Intervertebral disk tissue engineering using biphasic silk composite scaffolds. Tissue Eng Part A. 2012; 18:447–458. [PubMed: 21919790]
13. Nesti LJ, Li WJ, Shanti RM, Jiang YJ, Jackson W, Freedman BA, et al. Intervertebral disc tissue engineering using a novel hyaluronic acid-nanofibrous scaffold (HANFS) amalgam. Tissue Eng Part A. 2008; 14:1527–1537. [PubMed: 18707229]
14. Mizuno H, Roy AK, Zaporojan V, Vacanti CA, Ueda M, Bonassar LJ. Biomechanical and biochemical characterization of composite tissue-engineered intervertebral discs. Biomaterials. 2006; 27:362–370. [PubMed: 16165204]
15. Zhuang Y, Huang B, Li CQ, Liu LT, Pan Y, Zheng WJ, et al. Construction of tissue-engineered composite intervertebral disc and preliminary morphological and biochemical evaluation. Biochem Biophys Res Commun. 2011; 407:327–332. [PubMed: 21382343]
16. Mizuno H, Roy AK, Vacanti CA, Kojima K, Ueda M, Bonassar LJ. Tissue-engineered composites of anulus fibrosus and nucleus pulposus for intervertebral disc replacement. Spine (Phila Pa 1976). 2004; 29:1290–1297. discussion 7–8. [PubMed: 15187626]
17. Bowles RD, Gebhard HH, Hartl R, Bonassar LJ. Tissue-engineered intervertebral discs produce new matrix, maintain disc height, and restore biomechanical function to the rodent spine. Proc Natl Acad Sci U S A. 2011; 108:13106–13111. [PubMed: 21808048]
18. Bowles RD, Gebhard HH, Dyke JP, Ballon DJ, Tomasino A, Cunningham ME, et al. Image-based tissue engineering of a total intervertebral disc implant for restoration of function to the rat lumbar spine. NMR Biomed. 2012; 25:443–451. [PubMed: 21387440]
19. Holzapfel GA, Schulze-Bauer CA, Feigl G, Regitnig P. Single lamellar mechanics of the human lumbar anulus fibrosus. Biomech Model Mechanobiol. 2005; 3:125–140. [PubMed: 15778871]
20. Stokes IA. Surface strain on human intervertebral discs. J Orthop Res. 1987; 5:348–355. [PubMed: 3625358]
21. Nerurkar NL, Baker BM, Sen S, Wible EE, Elliott DM, Mauck RL. Nanofibrous biologic laminates replicate the form and function of the annulus fibrosus. Nat Mater. 2009; 8:986–992. [PubMed: 19855383]
22. Nerurkar NL, Elliott DM, Mauck RL. Mechanics of oriented electrospun nanofibrous scaffolds for annulus fibrosus tissue engineering. J Orthop Res. 2007; 25:1018–1028. [PubMed: 17457824]
23. Nerurkar NL, Mauck RL, Elliott DM. ISSLS prize winner: integrating theoretical and experimental methods for functional tissue engineering of the annulus fibrosus. Spine (Phila Pa 1976). 2008; 33:2691–2701. [PubMed: 19018251]
24. Nerurkar NL, Sen S, Huang AH, Elliott DM, Mauck RL. Engineered disc-like angle-ply structures for intervertebral disc replacement. Spine (Phila Pa 1976). 2010; 35:867–873. [PubMed: 20354467]

25. Nerurkar NL, Mauck RL, Elliott DM. Modeling interlamellar interactions in angle-ply biologic laminates for annulus fibrosus tissue engineering. Biomech Model Mechanobiol. 2011; 10:973–984. [PubMed: 21287395]
26. Baker BM, Shah RP, Huang AH, Mauck RL. Dynamic tensile loading improves the functional properties of mesenchymal stem cell-laden nanofiber-based fibrocartilage. Tissue Eng Part A. 2011; 17:1445–1455. [PubMed: 21247342]
27. Baker BM, Shah RP, Silverstein AM, Esterhai JL, Burdick JA, Mauck RL. Sacrificial nanofibrous composites provide instruction without impediment and enable functional tissue formation. Proc Natl Acad Sci U S A. 2012; 109:14176–14181. [PubMed: 22872864]
28. Driscoll TP, Nerurkar NL, Jacobs NT, Elliott DM, Mauck RL. Fiber angle and aspect ratio influence the shear mechanics of oriented electrospun nanofibrous scaffolds. J Mech Behav Biomed Mater. 2011; 4:1627–1636. [PubMed: 22098865]
29. Rousseau MA, Ulrich JA, Bass EC, Rodriguez AG, Liu JJ, Lotz JC. Stab incision for inducing intervertebral disc degeneration in the rat. Spine (Phila Pa 1976). 2007; 32:17–24. [PubMed: 17202887]
30. Gebhard H, James AR, Bowles RD, Dyke JP, Saleh T, Doty SP, et al. Biological intervertebral disc replacement: an in vivo model and comparison of two surgical techniques to approach the rat caudal disc. Evid Based Spine Care J. 2011; 2:29–35. [PubMed: 22956934]
31. Feng G, Zhang Z, Jin X, Hu J, Gupte MJ, Holzwarth JM, et al. Regenerating nucleus pulposus of the intervertebral disc using biodegradable nanofibrous polymer scaffolds. Tissue Eng Part A. 2012; 18:2231–2238. [PubMed: 22690837]
32. Baker BM, Nerurkar NL, Burdick JA, Elliott DM, Mauck RL. Fabrication and modeling of dynamic multipolymer nanofibrous scaffolds. J Biomech Eng. 2009; 131:101012. [PubMed: 19831482]
33. O'Connell GD, Vresilovic EJ, Elliott DM. Comparison of animals used in disc research to human lumbar disc geometry. Spine (Phila Pa 1976). 2007; 32:328–333. [PubMed: 17268264]
34. Beckstein JC, Sen S, Schaer TP, Vresilovic EJ, Elliott DM. Comparison of animal discs used in disc research to human lumbar disc: axial compression mechanics and glycosaminoglycan content. Spine (Phila Pa 1976). 2008; 33:E166–E173. [PubMed: 18344845]
35. Masuda K, Aota Y, Muehleman C, Imai Y, Okuma M, Thonar EJ, et al. A novel rabbit model of mild, reproducible disc degeneration by an anulus needle puncture: correlation between the degree of disc injury and radiological and histological appearances of disc degeneration. Spine (Phila Pa 1976). 2005; 30:5–14. [PubMed: 15626974]
36. Iatridis JC, Mente PL, Stokes IA, Aronsson DD, Alini M. Compression-induced changes in intervertebral disc properties in a rat tail model. Spine (Phila Pa 1976). 1999; 24:996–1002. [PubMed: 10332792]
37. Attia M, Santerre JP, Kandel RA. The response of annulus fibrosus cell to fibronectin-coated nanofibrous polyurethane-anionic dihydroxyoligomer scaffolds. Biomaterials. 2011; 32:450–460. [PubMed: 20880584]
38. Hudson KD, Mozia R, Bonassar LJ. Dose-dependent response of tissue engineered intervertebral discs to dynamic compressive loading. Transactions of the Annual Meeting of the Orthopaedic Research Society. 2013
39. Wuertz K, Godburn K, MacLean JJ, Barbir A, Donnelly JS, Roughley PJ, et al. In vivo remodeling of intervertebral discs in response to short- and long-term dynamic compression. J Orthop Res. 2009; 27:1235–1242. [PubMed: 19274755]
40. Korecki CL, Kuo CK, Tuan RS, Iatridis JC. Intervertebral disc cell response to dynamic compression is age and frequency dependent. J Orthop Res. 2009; 27:800–806. [PubMed: 19058142]
41. Mauck RL, Soltz MA, Wang CC, Wong DD, Chao PH, Valhmu WB, et al. Functional tissue engineering of articular cartilage through dynamic loading of chondrocyte-seeded agarose gels. J Biomech Eng. 2000; 122:252–260. [PubMed: 10923293]
42. Huang AH, Farrell MJ, Kim M, Mauck RL. Long-term dynamic loading improves the mechanical properties of chondrogenic mesenchymal stem cell-laden hydrogel. Eur Cell Mater. 2010; 19:72–85. [PubMed: 20186667]

43. Ionescu LC, Mauck RL. Porosity and cell preseeding influence electrospun scaffold maturation and meniscus integration in vitro. Tissue Eng Part A. 2013; 19:538–547. [PubMed: 22994398]
44. Baker BM, Gee AO, Metter RB, Nathan AS, Marklein RA, Burdick JA, et al. The potential to improve cell infiltration in composite fiber-aligned electrospun scaffolds by the selective removal of sacrificial fibers. Biomaterials. 2008; 29:2348–2358. [PubMed: 18313138]
45. Moffat KL, Kwei AS, Spalazzi JP, Doty SB, Levine WN, Lu HH. Novel nanofiber-based scaffold for rotator cuff repair and augmentation. Tissue Eng Part A. 2009; 15:115–126. [PubMed: 18788982]
46. Pham QP, Sharma U, Mikos AG. Electrospun poly(epsilon-caprolactone) microfiber and multilayer nanofiber/microfiber scaffolds: characterization of scaffolds and measurement of cellular infiltration. Biomacromolecules. 2006; 7:2796–2805. [PubMed: 17025355]
47. Burdick JA, Mauck RL, Gorman JH 3rd, Gorman RC. Acellular biomaterials: an evolving alternative to cell-based therapies. Sci Transl Med. 2013; 5:176ps4.
48. Rizza R, Liu X. Mechanics and validation of an in vivo device to apply torsional loading to caudal vertebrae. J Biomech Eng. 2013; 135:81003. [PubMed: 23722167]

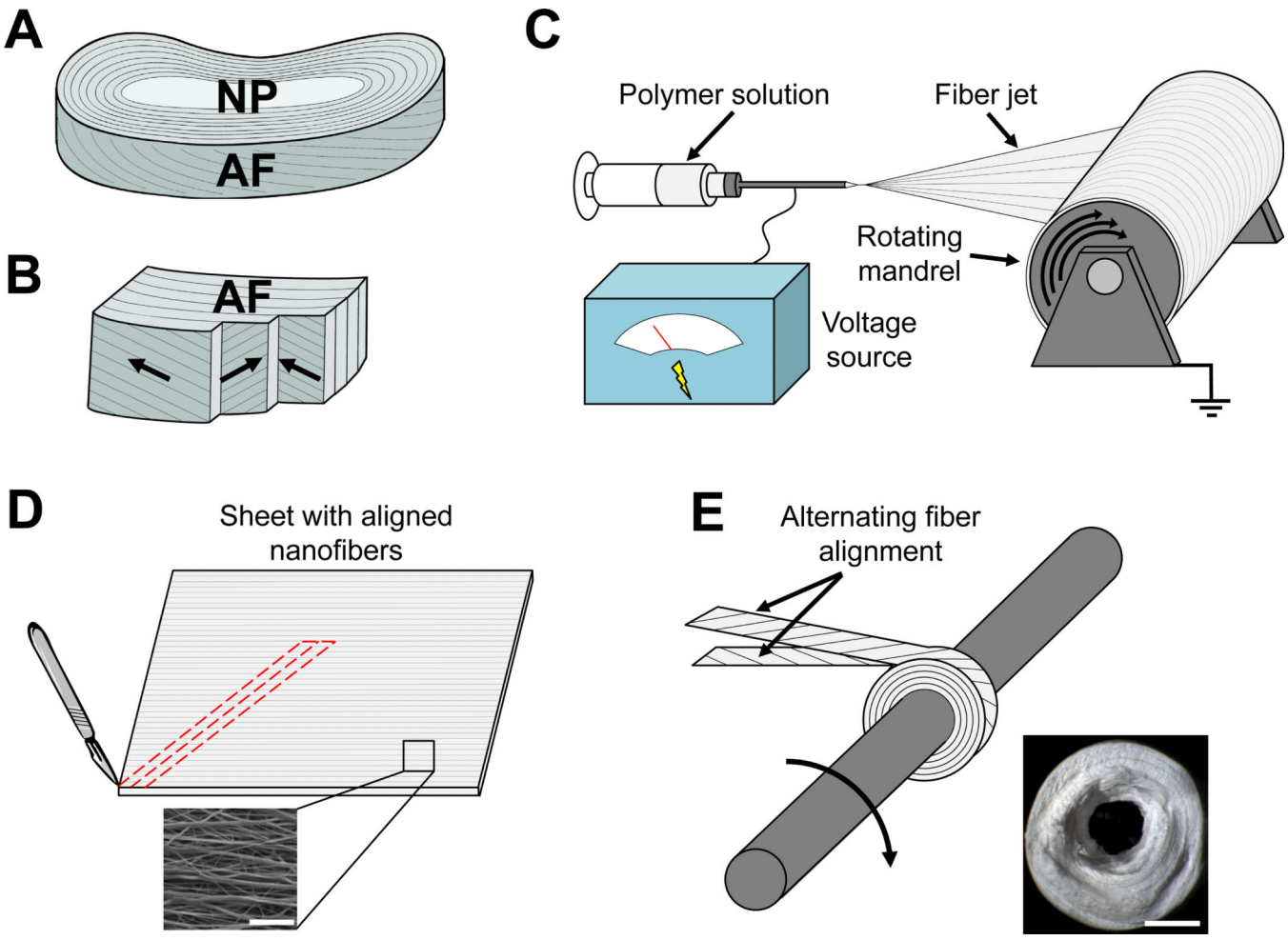

Fig. 1. Fabrication of disc-like angle ply structures (DAPS) that replicate the intervertebral disc lamellar patterning

(A) The intervertebral disc is a composite fibrocartilage that stabilizes multiaxial dynamic loading of the spine. It has two substructures that are targets for tissue engineering, the nucleus pulposus (NP) and the annulus fibrosus (AF). **(B)** The AF is composed of concentric lamellae with alternating +/− 30° collagen fiber alignment. **(C)** Single AF layers are replicated by electrospinning poly(ε-caprolactone) (PCL) nanofibers onto a rotating mandrel. **(D)** Aligned PCL nanofiber sheets **(bottom)** are then cut into strips at an angle **(top)** to establish a fiber arrangement consistent with native AF lamellae. **(E)** These strips are rolled about a post as bilayers with opposing fiber alignment **(top)** to form disc-like angle ply structures (DAPS) **(bottom)**. Scale = 10 μm in panel (D, bottom) and 1mm in panel (E, bottom).

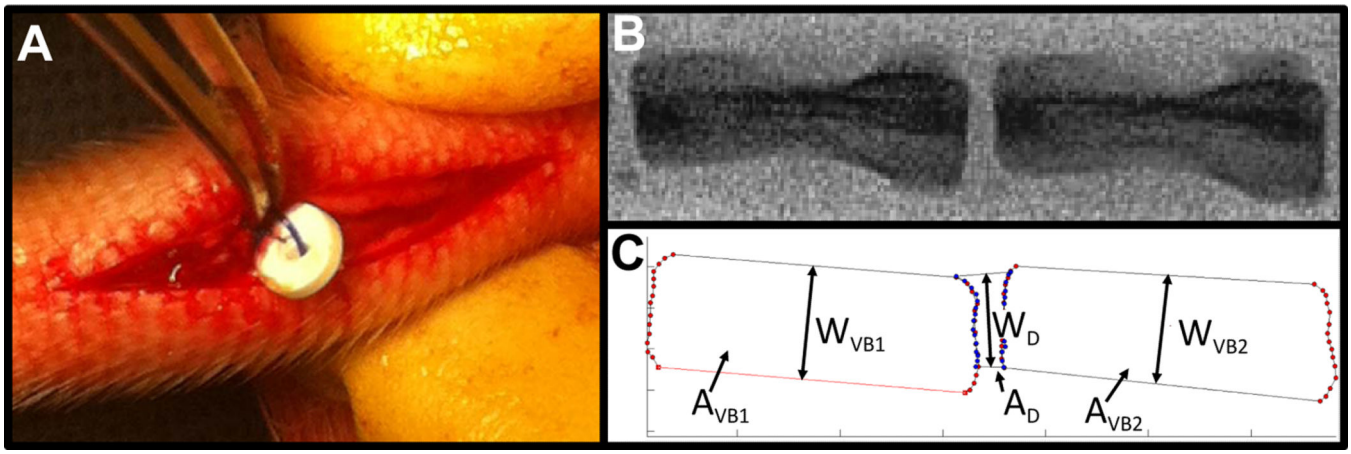

Fig. 2. DAPS implantation into the rat caudal spine and analysis of disc height

A rat tail model was used to evaluate DAPS integration and function. **(A)** Following a dorsal incision and discectomy, DAPS were implanted into the C8/C9 disc space and anchored to the ventral skin with a suture. **(B)** Lateral fluoroscopic images were taken at regular intervals throughout the study to analyze changes in disc height. **(C)** These changes were quantified through digital image analysis and expressed as Disc Height Index (DHI). The indicated quantities were used for calculating DHI: vertebral body 1 area, A_{VB1}, vertebral body 2 area, A_{VB2}, disc area, A_D, vertebral body 1 width, W_{VB1}, vertebral body 2 width, W_{VB2}, and disc width, W_D.

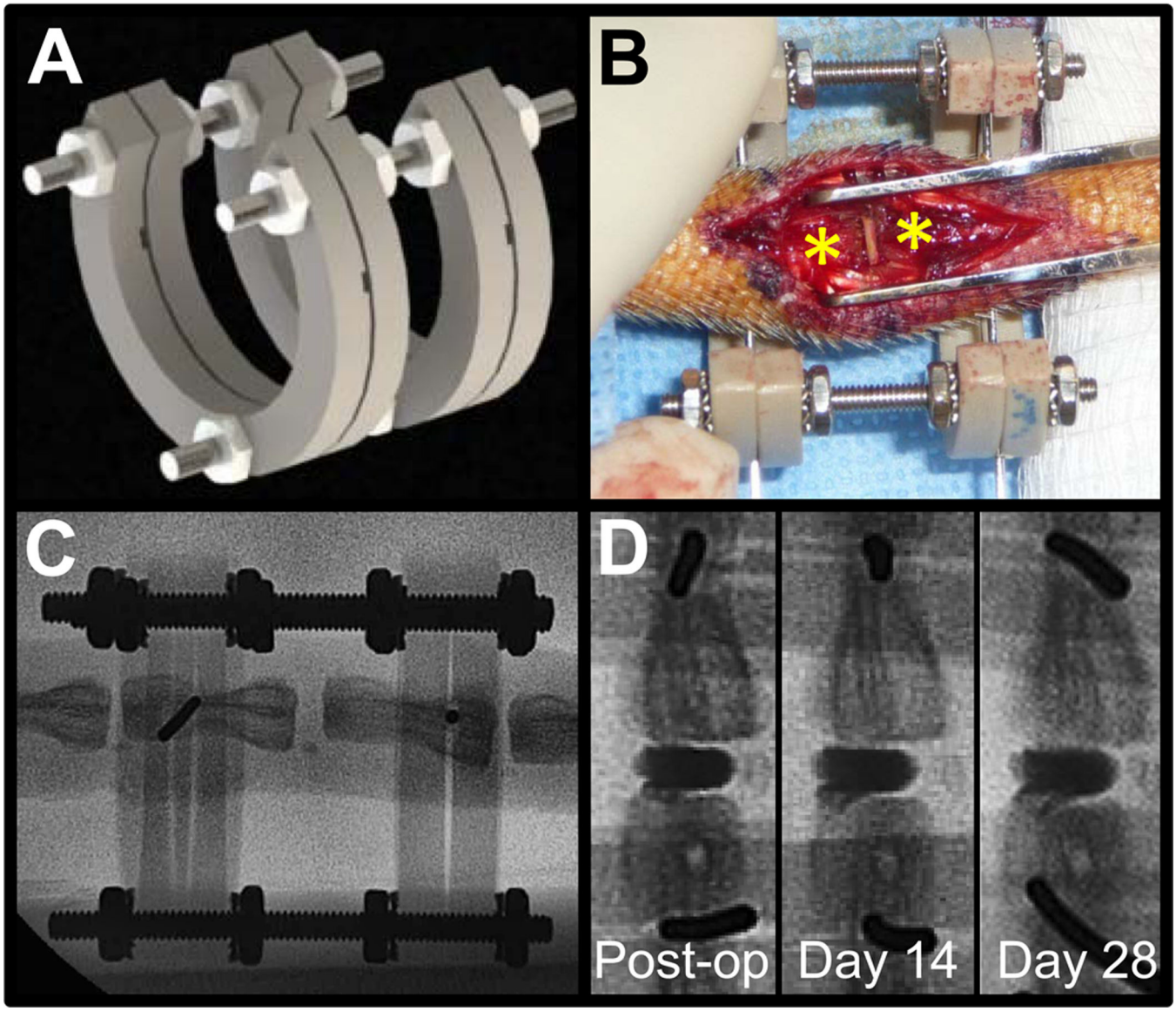

Fig. 3. External fixation to stabilize the caudal spine and improve DAPS retention

(A) Given observations of displaced implants following initial surgeries, an external fixator was designed to provide a stable environment for DAPS integration. **(B)** Surgical wires were passed through adjacent caudal vertebral bodies (*) and were inserted into machined grooves in the fixator. The open fixator design provided a window through which to conduct surgery. **(C)** The fixator ring material, PEEK, is radiolucent, allowing for visualization of the vertebral bodies by fluoroscopy and quantification of disc height over the course of the study. **(D)** Radiopaque DAPS (rDAPS) illustrate implant retention with external fixation over the course of 28 days.

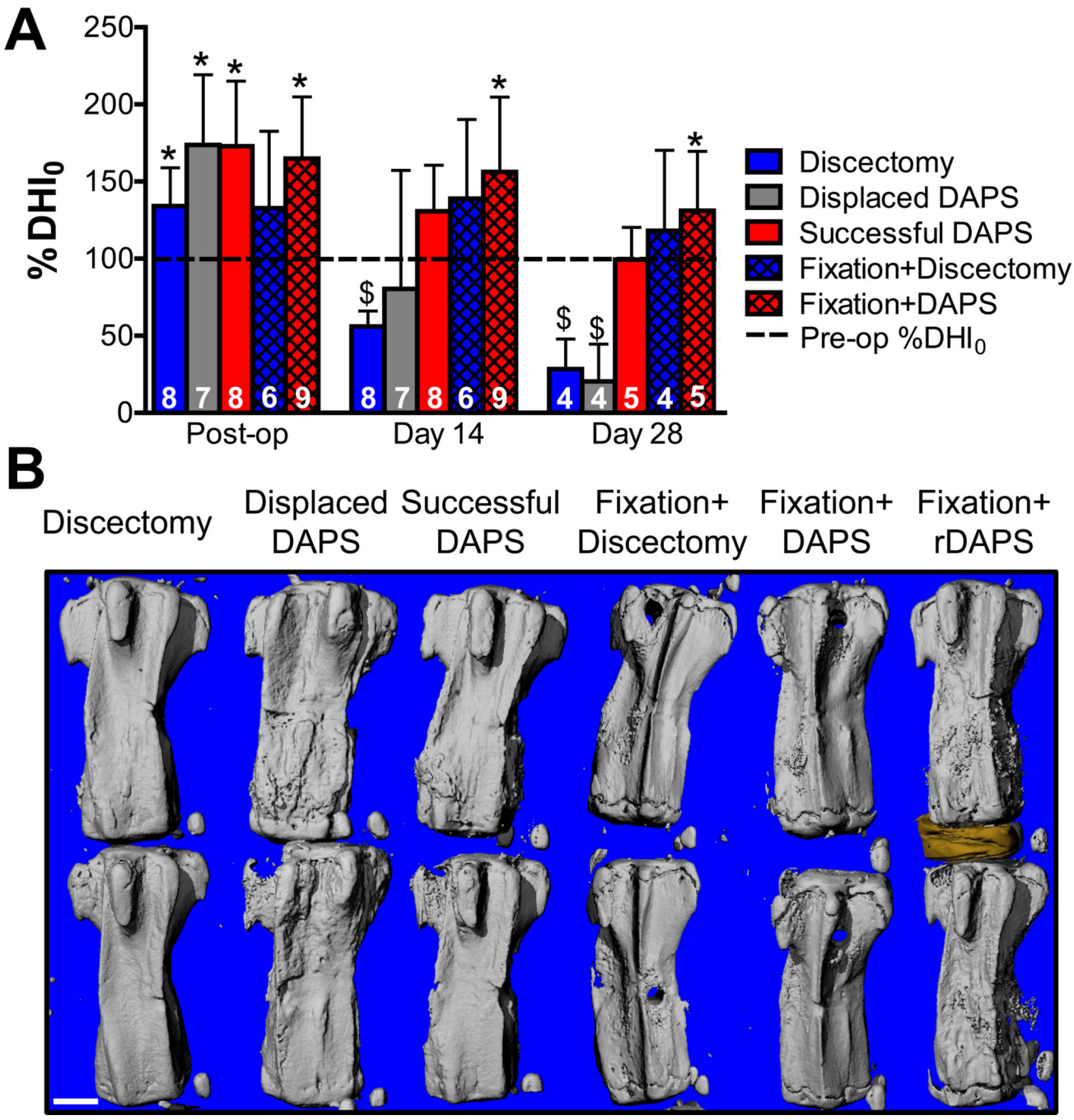

Fig. 4. DHI and bony anatomy for DAPS implantations with or without external fixation

(A) Flouroscopic analysis of $\%DHI_0$ for discectomy, displaced DAPS, successful DAPS, fixation+discectomy and fixation+DAPS surgeries over a 28 days. Significant differences ($p<0.05$) are displayed as (*, vs. pre-op) and ($, vs. successful DAPs, fixation+discectomy and fixation+DAPS groups). Sample numbers for each group are indicated at the base the corresponding bar. These decrease from day 14 to day 28 as rats were removed from the study (as scheduled) for μCT and histological analysis. For successful DAPS and both fixation groups, the pre-op disc height was maintained over the course of the study. For

DAPS that were eventually displaced, there was variation in the time at which they were displaced as evidenced by the large standard deviation at day 14. These eventually collapsed to a level similar the discectomy control group. **(B)** Representative μCT reconstructions for the same groups on day 28. Both discectomy and displaced DAPS groups collapsed by day 28, with the displaced DAPS group demonstrating new bone adjacent to the disc space. Disc height is maintained with little change in the bony architecture in the successful DAPS and both fixation groups. The rightmost panel shows the morphology of an implanted rDAPS and adjacent vertebrae. Scale = 2 mm.

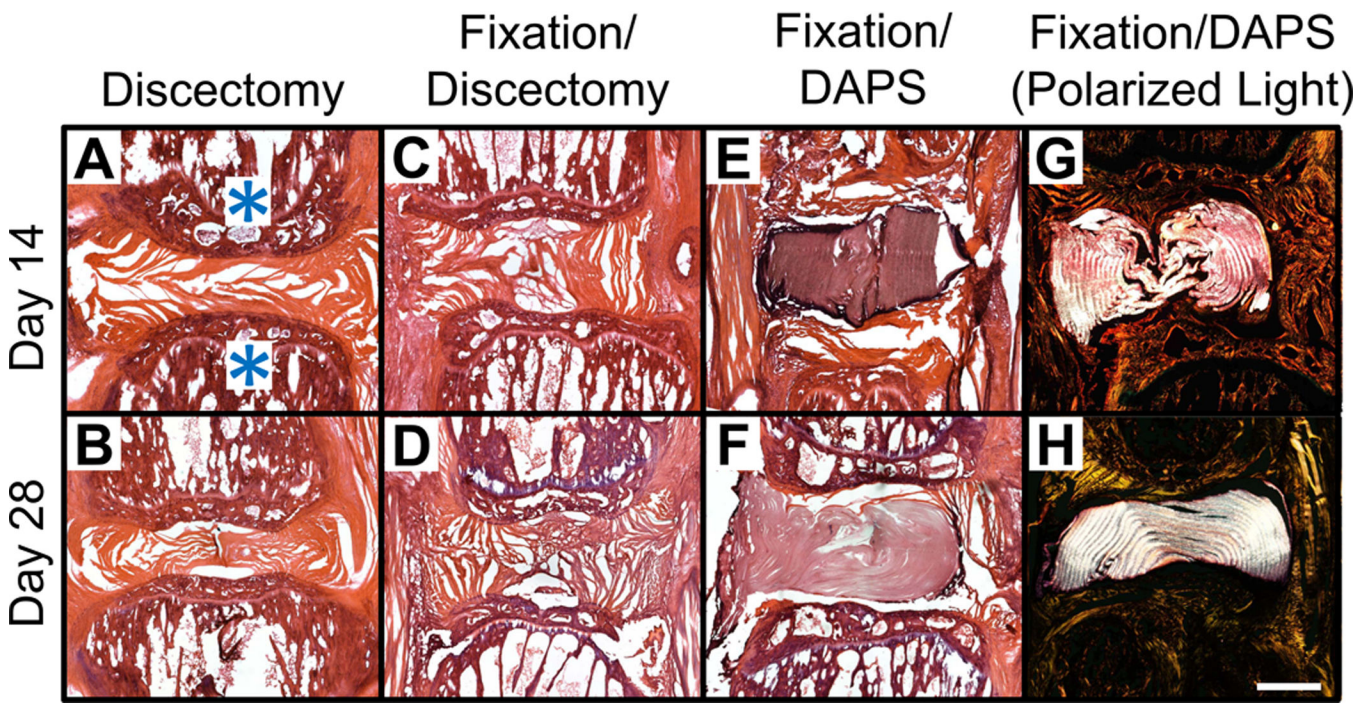

Figure 5. Histological appearance of DAPS in the rat caudal spine

Representative H&E stained sections at 14 and 28 days for discectomy **(A, B)**, fixation +discectomy **(C, D),** and fixation+DAPS groups **(E–H)**. Vertebral bodies are indicated by an asterisk (*) in (A). The fixation+DAPS group was imaged in both brightfield (E, F) and polarized light (G, H) to highlight the intact DAPS lamellar structure. The discectomy group showed narrowing of the disc space at both 14 and 28 days with some remnant AF visible. The fixation+discectomy group demonstrated an expanded disc space at day 14 that was maintained through day 28, and began to fill with fibrous repair tissue. In the fixation +DAPS group, the implant filled the disc space and, at 28 days, concentric lamellae with alternating fiber orientation were observed. Scale = 1 mm in panel (A).

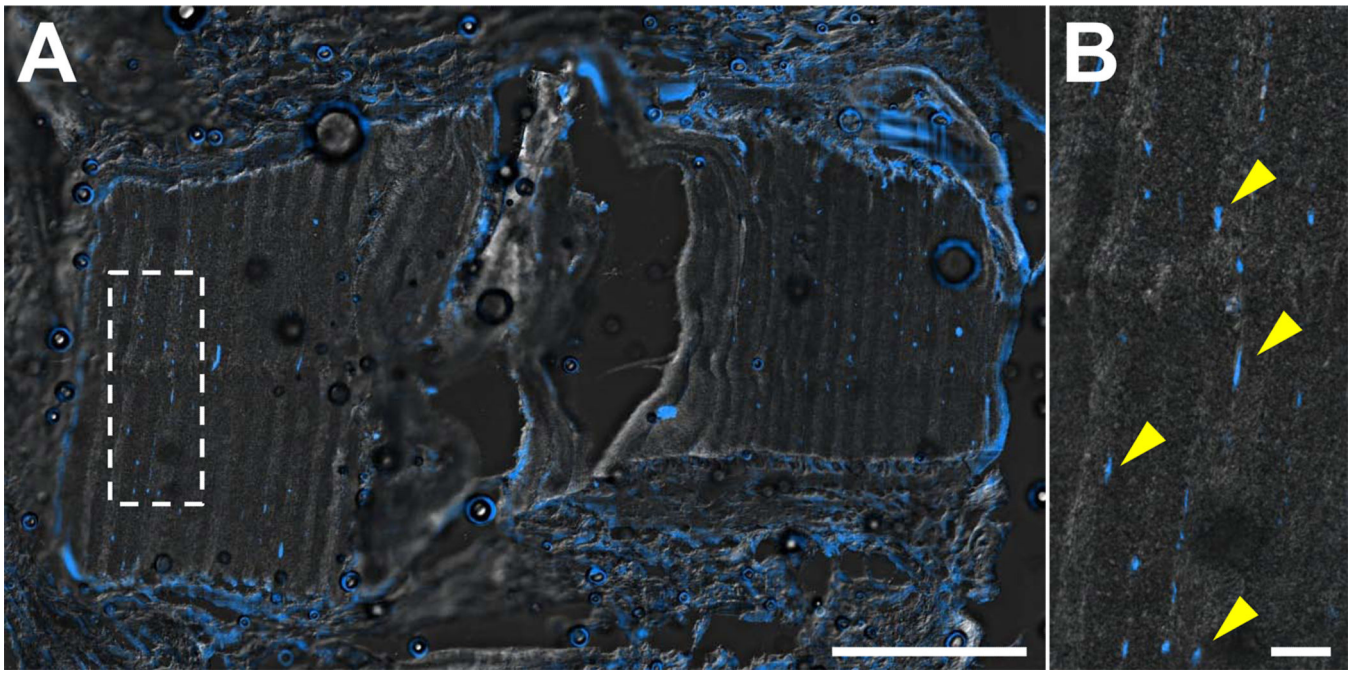

Figure 6. Cell infiltration into PCL-only DAPS *in vivo*

Representative DAPI staining of cell nuclei from a fixation+DAPS implant on day 28 at low magnification **(A)** and high magnification (inset) **(B)** overlaid with a DIC image of the DAPS structure. Cells aggregated at the periphery of the DAPS, with little infiltration into the DAPS layers. Cells that did populate the interlamellar space (arrows) had elongated nuclei, indicative of their orientation with the nanofiber template. Scale = 1mm in panel (A) and 100 μm in panel (B).

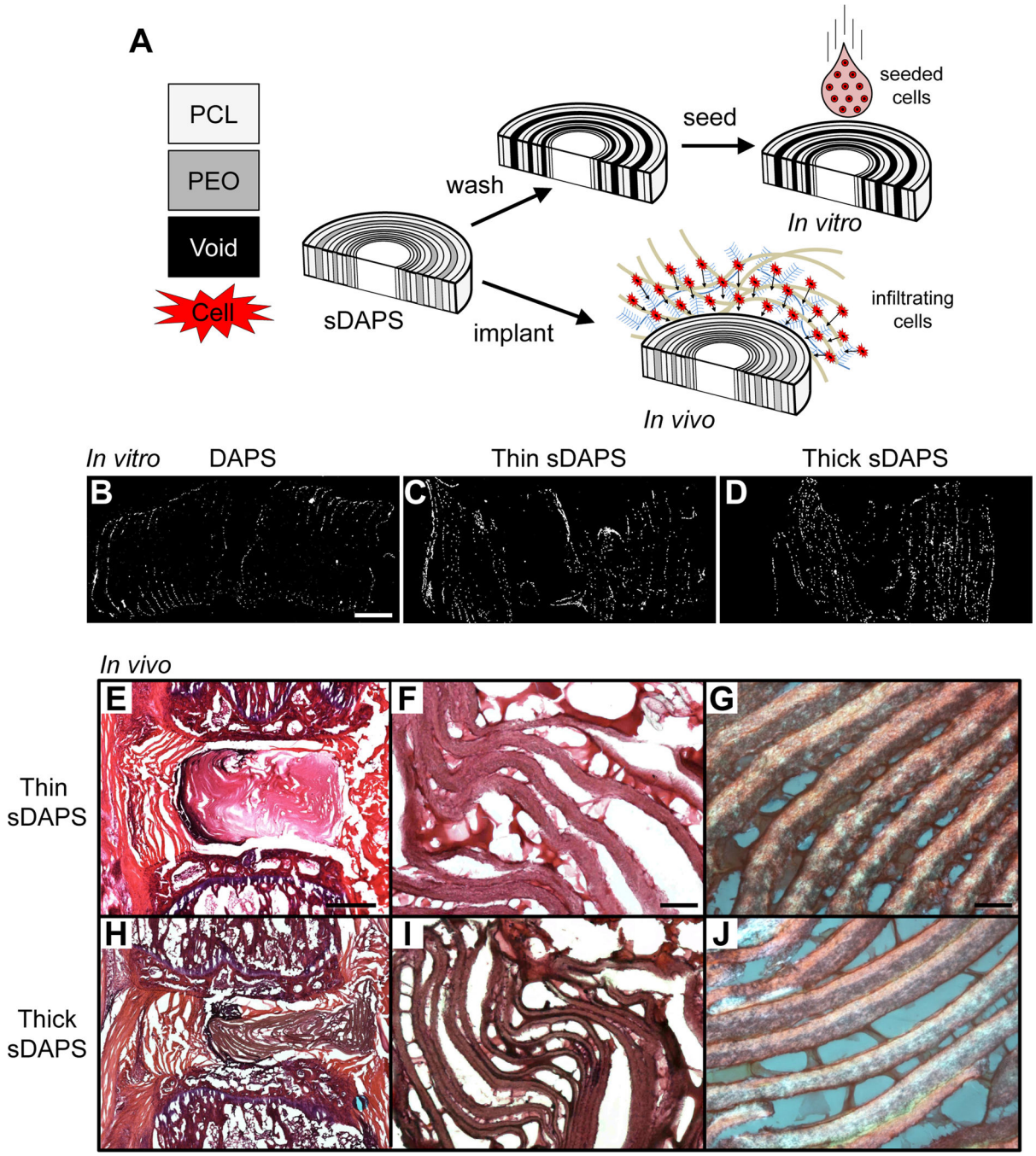

Figure 7. Sacrificial DAPS (sDAPS) improve cell colonization *in vitro* and *in vivo*

(A) To overcome issues of poor cell infiltration, sDAPS were fabricated with a layer of PEO spun directly onto a PCL layer prior to wrapping. sDAPS were evaluated both *in vitro* (via surface seeding of constructs with bovine AF cells and 7 days of culture) and *in vivo* (via direct implantation). DAPI staining of cross sections on day 7 show increasing cell infiltration *in vitro* comparing PCL-only DAPS **(B)**, 'thin' sacrificial layer sDAPS **(C)**, and 'thick' sacrificial layer sDAPS **(D)**. Implantation in the rat caudal spine (with external fixation) showed improved colonization and matrix deposition in 'thin' sDAPS **(E–G)** and

'thick' sDAPS **(H–J)**. Matrix formation between lamellae was apparent at higher magnification in both formulations (F, G and I, J). Scale = 500 μm in (B), 1 mm in panel (E), 100 μm in panel (F), and 50 μm in panel (G).